

# FORTE: Tactile Force and Slip Sensing on Compliant Fingers for Delicate Manipulation

Siqi Shang, Mingyo Seo, Yuke Zhu, and Lillian Chin

**Abstract**—Handling delicate and fragile objects remains a major challenge for robotic manipulation, especially for rigid parallel grippers. While the simplicity and versatility of parallel grippers have led to widespread adoption, these grippers are limited by their heavy reliance on visual feedback. Tactile sensing and soft robotics can add responsiveness and compliance. However, existing methods typically involve high integration complexity or suffer from slow response times. In this work, we introduce FORTE, a tactile sensing system embedded in compliant gripper fingers. FORTE uses 3D-printed fin-ray grippers with internal air channels to provide low-latency force and slip feedback. FORTE applies just enough force to grasp objects without damaging them, while remaining easy to fabricate and integrate. We find that FORTE can accurately estimate grasping forces from 0–8 N with an average error of 0.2 N, and detect slip events within 100 ms of occurring. We demonstrate FORTE’s ability to grasp a wide range of slippery, fragile, and deformable objects. In particular, FORTE grasps fragile objects like raspberries and potato chips with a 98.6% success rate, and achieves 93% accuracy in detecting slip events. These results highlight FORTE’s potential as a robust and practical solution for enabling delicate robotic manipulation. Project page: <https://merge-lab.github.io/FORTE>

**Index Terms**—Tactile Sensing, Soft Robotics, Robotic Manipulation, Slip Detection

## I. INTRODUCTION

MIMICKING the delicate manipulation capabilities of humans has been a longstanding goal of the robotic manipulation community. Humans can precisely control the interaction forces they apply to delicate and fragile objects, modulating just 0–5 N of force across any object shape or geometry [1], [2]. To avoid damaging the grasped object, humans must apply just enough force to prevent the grasped object from slipping without applying any excess force that deforms or marks the object [3]. Humans are able to balance this tradeoff through the mechanoreceptors embedded within our skin, which provide accurate force and slip information in real-time [4]–[7].

Despite not having the same dexterous fingers and hardware as humans, current robots can complete a wide range of manipulation tasks. Rigid parallel grippers remain the most popular option for deployment due to their simplicity and have been shown to be capable of performing tasks as varied

This work was partially supported by the Texas Robotics Industrial Affiliate Program, the National Science Foundation (FRR-2145283, EFRI-2318065), the Office of Naval Research (N00014-24-1-2550), the DARPA TIAMAT program (HR0011-24-9-0428), and the Institute of Information & Communications Technology Planning & Evaluation (IITP) grant funded by the Korean Government (MSIT) (No. RS-2024-00457882, National AI Research Lab Project).

All authors are with The University of Texas at Austin, TX, USA. Correspondence: [siqi.shang@utexas.edu](mailto:siqi.shang@utexas.edu)

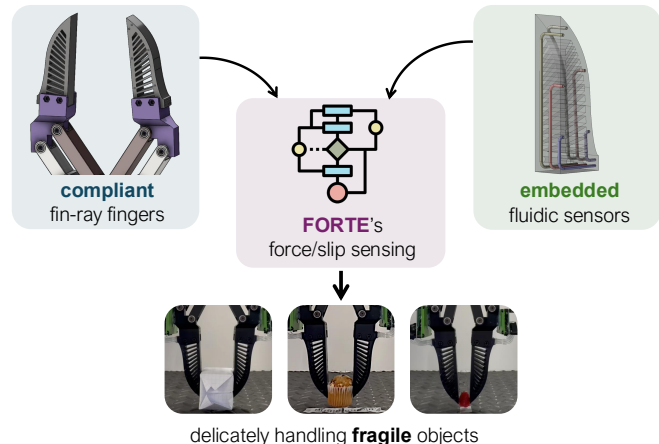


Fig. 1. **Overview.** FORTE enables the delicate manipulation of fragile objects by leveraging passive compliance and tactile feedback. This is achieved by integrating compliant fin-ray fingers and embedded fluidic sensors with algorithms for force estimation and slip detection.

as laundry folding to loading a dish rack [8]–[11]. However, with this simplicity comes a fundamental challenge: the lack of direct grasp feedback. Unlike humans, most robots with parallel grippers rely solely on visual feedback and perform only binary actions [12] or simplified open-close control of gripper width [13]–[15]. This limits the extent to which these rigid grippers can safely grasp fragile objects.

Robotics researchers have realized this gap and have improved rigid parallel grippers with two approaches: (1) adding compliance to the fingers, and (2) incorporating tactile sensors into the fingertips. In the former approach, researchers have adopted designs like the Fin-ray gripper [16] so binary open-close actions deform the gripper rather than the object. However, this passive deformation makes precise force control difficult, making it challenging to handle objects with varying fragility [16], [17]. In the latter approach, researchers add tactile sensors to existing grippers [18], [19]. While effective, these sensors tend to either be expensive off-the-shelf sensors with durability issues [20]–[23] or custom sensor technologies with complex fabrication or signal processing requirements [24]–[28]. A simple end-effector design that incorporates force and slip sensing in a compliant gripper would be a significant step towards achieving human-like delicate manipulation capabilities.

In this paper, we introduce FORTE (Fragile Object Grasping with Tactile Sensing), a tactile force and slip sensing system embedded in compliant fingers for delicate manipulation. We address the issues involved in previous sensorized compliant fingers by combining the core technologies of fin-ray-style

fingers and fluidic innervation (Figure 1). Both of these technologies are easily manufacturable through common 3D-printing techniques, making it easy for other researchers to extend our work. Instead of mounting external tactile sensors, FORTE leverages internal air channels embedded within the compliant finger structure for sensing. The internal channels deform as the finger deforms, providing a pressure signal that can be read by the off-the-shelf transducer. Since the force signals directly follow from the gripper’s internal deformation, FORTE circumvents many of the interface and robustness challenges inherent to previous tactile sensor solutions. The sensor signals provide an accurate reflection of the physical interaction between the gripper and the object, enabling precise force estimation. Their fast response and high temporal resolution enable a frequency-domain analysis of tactile signals, allowing reliable slip detection between the gripper and the object. FORTE enables the robot to grasp a wide range of fragile, slippery, and deformable objects with a 91.9% success rate across 310 trials. Akin to human grasping, FORTE applies just the right amount of force to grasp delicate objects and dynamically adds more force if the object slips. We make the following contributions in this work:

- We design and manufacture compliant fingers with internal air channels for sensing. The fingers sense contact events with a high sampling rate of 2 kHz.
- We achieve accurate force estimation with validation RMSE below 0.2 N.
- We develop a novel analytical slip detection algorithm that achieves 0.91 overall F1 score on 31 items with 29 unseen.
- We demonstrate FORTE’s capability for precise force estimation and slip detection through single-trial grasps of 31 different items, achieving a 91.9% success rate.
- We publicly release the hardware designs and algorithmic implementations at <https://merge-lab.github.io/FORTE>.

## II. BACKGROUND

In this section, we compare FORTE against other tactile sensing solutions for compliant grippers to contextualize our design approach. We also provide a brief summary of slip detection and its application in robotic manipulation. Slip detection is a relatively underexplored and non-standardized area in robotic manipulation, requiring additional justification for our characterization procedures.

### A. Compliant Grippers with Tactile Feedback

To incorporate tactile sensing in a compliant gripper, roboticians must consider whether the tactile sensor will add unwanted stiffness to the soft gripper. A tactile sensor with a rigid backing will add a stiff patch, and the gripper will no longer be compliant. Typical off-the-shelf tactile sensor types that are compatible with compliant grippers include vision-based [20]–[23], [29], [30], acoustic [31]–[33], and barometric [34]–[36].

Vision-based tactile sensing is a widely adopted approach for compliant grippers as it offers a non-intrusive way to

preserve structural compliance. These sensors consist of a soft elastomeric surface backed by an internal camera, enabling high-resolution measurement of surface deformations. A common integration with compliant grippers involves hollowing out the finger to embed cameras, which provide rich contact information [20]–[22], [29], [30]. However, the internal camera introduces additional fabrication difficulties and limits structural simplicity. Moreover, these sensors typically require a soft, deformable surface to produce high-resolution contact profiles. This surface is often *too* compliant and tears under repeated / high-force interactions.

Acoustic tactile sensors also preserve structural compliance as microphones can be embedded underneath the contact surface of the finger. The high-frequency acoustic signals captured by a microphone enable contact force and location sensing [31], material identification [32], and contact-rich policy learning [33]. However, their performance can be limited by environmental noise and the complexity of interpreting signals under compliant contact.

Finally, barometric solutions work by adding internal air chambers to the soft fingers. Since air is a compressible fluid, these empty air chambers will not only match the softness of the structure, but also have a measurable pressure change as the fingers deform. With rigid electronic components fully off-loaded from the sensing site, a barometric structure can maintain robustness under 100% elongation, detect dynamic contact events such as object sliding, and enable simultaneous contact localization, force sensing, and delicate in-hand manipulation [34], [37], [38]. However, these solutions often involve complex design and fabrication processes, which can introduce sensor noise and compromise long-term durability. Fluidic innervation alleviates this limitation of traditional barometric sensing by 3D printing the finger structure with embedded internal air channels. With only 12 sensors, a sensorized gripper can estimate an object’s weight and location and offer new insights into grasp parameters like friction coefficients and grasp force [35], [36]. However, this method has not been demonstrated across a wide range of objects or in more complex soft robotic grippers.

In this work, we apply fluidic innervation to the fin-ray gripper. This approach avoids the durability and fabrication challenges of vision-based sensors and eschews the complex signal processing requirements of acoustic-based sensors. Our 3D-printing-based method results in easy fabrication and results in precise force estimation and slip detection capabilities.

### B. Slip Definition and Detection

In robotic grasping, slip events are broadly classified into two types: gross slip and incipient slip [19], [39]. Gross slip refers to relative motion occurring across the entire contact interface between two surfaces. Incipient slip describes the partial slip that initiates within the contact area while the rest remains stationary. A slip event typically starts with incipient slip, when external forces overcome local static friction and cause relative motion within the contact area. In a parallel gripper scenario, if a slip appears only at one finger, this is also considered an incipient slip.

In addition to these general categories, slip can also be classified by the type of relative motion between the contacting surfaces:

- **Translational:** relative linear motion between contacting surfaces along the tangential direction.
- **Rotational:** relative angular motion between contacting surfaces around the normal axis.
- **Stick-Slip:** the alternating motion between static friction contact and sudden slipping [40].

To identify slip events during grasping, two major methods have emerged: (1) detecting relative motion at the contact surface and (2) sensing vibrations induced by slip events. To detect relative object motion at the end-effector surface, the most common approach is to use vision-based tactile sensors to track the displacement of contact textures or embedded markers. These methods can reliably detect both translational and rotational incipient slip with high spatial precision [41], [42]. A downside of this method is that it typically requires a large normal force to produce a clear and well-defined contact profile for evaluating relative motion. For example, 50 N of pressure force is required to effectively detect the slip of a crayon box and sponge [41]. This level of force is infeasible for delicate manipulation. To improve temporal resolution, several studies have replaced the internal RGB camera in vision-based tactile sensors with event-based cameras operating at sampling rates up to 1 kHz [43]–[45]. By tracking the markers imprinted in the gel surface, a learned prediction model can detect slip events across different objects in real-time [45]. However, they remain constrained by the durability limitations common to vision-based tactile solutions. Unlike high-dimensional vision-based methods that often rely on data-driven models, our approach directly measures finger deformation with higher sensitivity, enabling a physically grounded and analytically tractable slip detection algorithm for delicate manipulation.

Vibration-based methods detect slip events by identifying high-frequency signals caused by micro-movements at the contact interface. The most common method is setting a threshold on the signal power within specific frequency bands, using power peaks as indicators of slip events [46]–[50]. This method is difficult to generalize because of its high sensitivity to noise and the highly variable sensor response from different combinations of surface properties of the fingers and objects [19]. A more reliable alternative is to use the magnitude of the tangential force derivative as the target feature for slip detection [48]. While effective, this method depends on accurate tangential force sensing. The additional latency from force estimation may hinder timely slip detection. Finally, learning-based methods have been explored for detecting the vibrations induced during slip [51]–[53]. Despite their success, these methods often suffer from limited generalizability and interpretability, which are common challenges in neural network approaches. In particular, generating comprehensive datasets of diverse slip events remains challenging to automate and scale. In this paper, we address these issues with an analytical slip detection algorithm using the second-order moving variance of signal power as the target feature. Our method can effectively capture stick-slip events without additional

algorithmic dependencies or special hardware.

### C. Experimentally Characterizing Slip

Despite its importance, there are no standardized techniques for evaluating object slip in a robot grasp. We provide a brief literature review of how other researchers created artificial slips for characterization to justify our approach in Section IV-B.

The most common method of generating slip events is to fix the tactile sensor and then generate planar displacement between the object and sensor [20], [46], [54], [55]. In this setting, the relative motion is fully under control for one sensor, but the uneven force distribution between fingers and the objects is difficult to replicate. This method also inherently constrains the motion to be planar, which is rarely the case for real-world grasps. Indeed, we noted many non-planar tangential tilts in Figure 5a and Section IV-B.

Another popular method adopted involves a human operator generating slip events by manually pulling objects out of a robot grasp [56], [57]. While efficient for scaling up data collection, the collected slip events could be biased due to two limitations. First, the interaction forces created by the human operator can have arbitrary direction and magnitude, potentially deviating from force patterns in real-world slips. Second, the generated slip events typically occur at higher gripping forces, as the object starts securely grasped before being forcibly removed. This differs fundamentally from natural slip scenarios, which arise due to insufficient gripping force, and may lead to different slip responses.

The final method for generating slip events is to first grasp the object off the ground, and then gradually open the gripper until the object drops [48]. While this allows for unconstrained non-planar object motion, we may lose characterization of the lower range of gripping force, as the object may already be dropping out of grasp.

To address these concerns, we choose to characterize slip in Section IV-B by lifting objects from the tabletop starting from a very low grasping force. We believe lifting an object is most suitable for evaluating the slip detection performance of grippers since the object motion is unconstrained and a larger range of grasp forces can be covered [42].

## III. METHODS

To achieve delicate manipulation of fragile objects, we design FORTE by combining three elements into one complete package: mechanical design, sensorization, and algorithms (Figure 1). In this section, we discuss how each of these three elements contributes to FORTE’s ability to estimate force and detect slip.

### A. Hardware Design

We design FORTE’s fingers based on the fin-ray fingers [16]. Fin-ray structures are a popular manipulator design as their geometric structure creates a tight conformation to the object when deformed. This deformation maximizes contact surface area and creates a tight and secure grasp [58], [59].

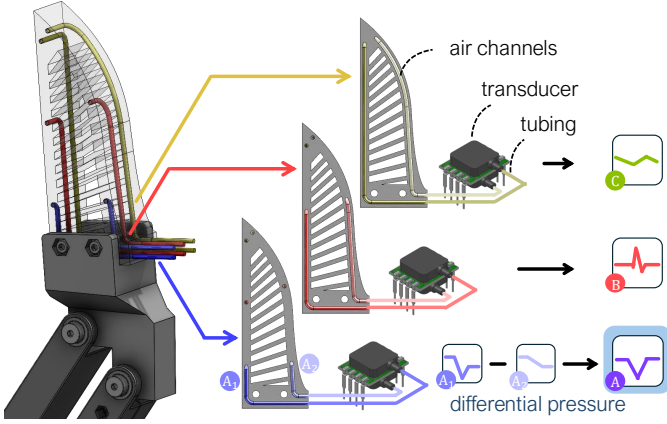


Fig. 2. **Hardware Design of FORTE.** Fin-ray fingers with internal empty air channels are 3D printed as a single structure. The empty air channels act as a fluidic tactile sensor by measuring their pressure with an off-the-shelf pressure transducer. The channels are L-shaped and evenly distributed to sensorize the entire finger. Each pair of channels (marked as the same color) under the inner and outer surfaces of the finger is sealed on the side surface and connected to one differential air pressure transducer.

However, this large deformation also makes it challenging to seamlessly incorporate tactile sensing without hampering the compliant deformation (Section II-A).

We pair fin-rays with fluidic innervation, a sensorization technique that works by measuring the air pressure of an empty air channel embedded within a 3D-printed structure [35], [36]. As the structure deforms or compresses, the air channels deform as well. This resulting change in air pressure can be measured with off-the-shelf pressure transducers. As fluidic innervation does not change a structure’s overall geometry, we can preserve the fin-ray’s high deformation with the sensitivity of fluidic innervation.

We print the fin-rays out of EPU 40 on a Carbon M2 printer with the air channels embedded under the inner and outer surface of the finger (Figure 2), following the protocol in Truby et. al [35]. For design, we follow a similar design principle as Zhang et. al. [36]. We design our channels in an L-shape to cover the surface of the fingers while also capturing vertical and horizontal information. Each channel has a diameter of 2 mm, with a 1 mm-thick wall between the channels and the adjacent surface. To simplify the connection to the pressure transducers, the channels end at the back surface of the finger. The distal ends of the channels are all along the side surface of the fingers and are sealed with silicone epoxy (Sil-Poxy, Smooth-On). Each transducer (All Sensors ELVR-L01D, operating range of 1 inH<sub>2</sub>O) is connected to the corresponding inner/outer channels in the finger via silicone tubing, which we keep as short as possible to avoid the risk of sensor drift (< 4 cm). Since each pressure transducer measures the *difference* in pressure, each transducer measures the *net* pressure change between the two channels in the pair.

Each finger is sensorized with 3 transducers, resulting in 6 sensor signals total across FORTE. The sensor patterns are a mirror copy of one another. This symmetry helps us identify the dynamic effects arising from physical imbalance, such as slippage resulting from uneven force distribution (Figure 5a).

The transducers are connected to the analog inputs of an ESP32-S3 and sampled at 2 kHz at an 11-bit resolution to capture rapid and transient dynamics that occur over short time scales. The analog readings are normalized to the range of  $-1$  to  $1$  and transmitted at 2 kHz to a host PC. The sensor signals are filtered with a median filter of size 11 to reduce impulsive noise while preserving transient features, inducing at most 2.5 ms of latency.

### B. Force Estimation

Since the pressure transducers directly measure the pressure difference between the inside and outside channels of the finger, we can estimate the gripping force directly from the filtered sensor readings. We employ Support Vector Regression (SVR) with a radial basis function (RBF) kernel. To account for sensor drifting and stress relaxation effects, three additional features are introduced for each channel, representing the mean values of the most recent 2.5, 5, and 10 seconds of historical data, or 5k, 10k, and 20k datapoints.

Let the sensor signal frame at time  $t$  be  $S(t) \in \mathbb{R}^6$ , and the sensor sampling frequency be  $f_s$ . The feature vector  $z(t)$  is defined as:

$$z(t) = \bar{S}_{2.5}(t) \oplus \bar{S}_5(t) \oplus \bar{S}_{10}(t)$$

where  $\bar{S}_\tau(t) \in \mathbb{R}^6$  denotes the mean of the past  $\tau$  seconds of sensor data. The most recent sensor frame  $S(t)$  is concatenated with the feature vector  $z(t)$  to form an input vector  $v = S(t) \oplus z(t) \in \mathbb{R}^{24}$ . We use  $v$  as input to our SVR model to estimate the actual grip force.

### C. Slip Detection

The high temporal resolution of the sensors means that we can not only estimate grasping force, but also track transient changes in the applied force over time. This allows us to detect when the object slips from a grasp.

Based on previous work on vibration-based methods for slip detection [46]–[50], we make the following assumptions for our method. First, we hypothesize that slip events produce a sudden emergence of high-magnitude features in the frequency domain of the pressure sensor signal. Second, we hypothesize that such features are exclusive to slip and do not appear during other types of contact interaction. Rather than detecting individual power peaks, our method tracks the increase in spectral power within a specific frequency band as a more effective feature.

To detect slip, we analyze the Power Spectral Density (PSD) of  $S(t)$  in the frequency domain, apply windows to measure the moving variance across our sensor feature’s history, and threshold the results into a binary variable  $\eta \in \{0, 1\}$  indicating slip.

First, we apply a Discrete Fourier Transform to the sensor signal  $S_i(t)$  for a given sensor index  $i$ . We then divide the frequency-domain signal into  $K$  overlapping windows of length  $N$  with step  $N - O \cdot N$ , where  $O$  is the overlap factor. For each segment  $k$ , the sensor  $i$ ’s signal is first windowed and then transformed into the frequency domain to obtain

$$X_{i,k}(f) = \sum_n x_i(n)w(n)e^{-j2\pi fn}, \quad (1)$$

where  $x_i(n) = S_i\left(t_k - \frac{N-1-n}{f_s}\right)$  with  $n = 0, 1, \dots, N-1$  indexing the  $N$  samples of segment  $k$  ending at time  $t_k$ ,  $w(n)$  is the Hann window function, and  $j = \sqrt{-1}$ . Thus, the sensor signal of segment  $k$  for sensor  $i$  is implicitly present in  $X_{i,k}(f)$ .

The expression  $|X_{i,k}(f)|^2$  gives an estimate of the power at frequency  $f$  for that segment, and normalizing these values yields the power spectral density  $P_i(f)$  for sensor  $i$  in the unit of  $(\text{inH}_2\text{O})^2/\text{Hz}$ . For each sensor  $i$  and the most recent window  $x$ , we compute the PSD  $P_i$  for normalized frequency  $f_k = \frac{k}{N}$ ,  $0 \leq k < N$  using Welch's method as:

$$P_i(f_k) = \frac{1}{f_s \sum_{n=0}^{N-1} w^2(n)} \left| X_{i,k}\left(\frac{k}{N}\right) \right|^2. \quad (2)$$

For each sensor's computed PSD, we select the maximum value across its frequency bins to form a scalar feature. We define this PSD feature as:

$$P_i^{\max} = \max_{f \in [f_{\min}, f_{\max}]} \left\{ 10 \log_{10}(P_i(f) + \epsilon) \right\}. \quad (3)$$

We add a small constant  $\epsilon = 1 \times 10^{-12}$  to the power spectral density estimate before taking the logarithm to prevent numerical stability of potentially taking  $\log 0$ . The PSD feature represents the maximum value of power magnitude within the selected frequency range  $[f_{\min}, f_{\max}]$ .

To quantify temporal fluctuations in spectral power and search for our large-magnitude frequency feature, we compute the moving variance of the PSD magnitude as a second-order statistical feature. For each sensor  $i$ , we create a double-ended queue of  $P_i^{\max}$  as a history  $H_i$ , which has a fixed length  $V$ . We then compute the moving variance over the feature history:

$$\sigma_i^2 = \begin{cases} \text{Var}(H_i), & \text{if } H_i(k+1) - H_i(k) > \delta, \forall k, \\ 0, & \text{otherwise.} \end{cases} \quad (4)$$

Each sensor  $i$  belongs to either the right finger or the left finger. To detect slip at the finger level, we average the moving variance across the entire finger, which also helps reduce the impact of sensor noise. Let the finger group  $G$  denote the set  $\{R, L\}$  for the right and left fingers, respectively. The average moving variance is:

$$\bar{\sigma}_g = \begin{cases} \frac{1}{|g|} \sum_{i \in g} \sigma_i^2, & \text{if } \bar{\sigma}_g \geq \alpha, \forall g \in G, \\ 0, & \text{otherwise.} \end{cases} \quad (5)$$

Finally, we define the slip indicator  $\eta$  as whether either finger passes some max pre-defined threshold  $T$ .

$$\eta = \begin{cases} 1, & \text{if } \max_{g \in G} \bar{\sigma}_g > T, \\ 0, & \text{otherwise.} \end{cases}$$

We summarize the selected parameter values we use for FORTE in Table I. For segments with  $N = 400$  and  $f_s = 2$  kHz, the frequency resolution of the resulting PSD is 5 Hz. Together with the selected frequency band of  $[10, 50]$  Hz, the FFT bins span the frequency range  $[7.5, 52.5]$  Hz. The frequency range is selected to approximate that of fast-adapting

TABLE I  
SLIP DETECTION PARAMETERS

Parameter	Value
Median filter window size	$M = 11$
FFT window size	$N = 400$
Overlap	$O = 0.99$
Frequency band	$[f_{\min}, f_{\max}] = [10, 50]$ Hz
PSD history length (moving window size)	$V = 15$
Minimal increment for monotonicity	$\delta = 0.1$ dB
Minimum group average variance	$\alpha = 0.6$ dB <sup>2</sup>
Slip detection threshold	$T = 2$ dB <sup>2</sup>

type I (FA-I) mechanoreceptors in the human hand, which are known to reliably encode frictional slip events during object manipulation [7]. With the selected window size  $N = 400$  and overlap factor  $O = 0.99$ , the step size of the sliding window is 4, resulting in a slip detection frequency of 500 Hz. With a PSD history of length  $V = 15$ , the moving variance is calculated with PSD features of the last 30 ms, which is sufficient to capture temporal trends while maintaining a timely response.

#### IV. CHARACTERIZATION

In this section, we characterize FORTE's ability to estimate grip force and detect slip during an attempted grasp. For force estimation, we focus on accuracy in low-force regimes relevant to delicate manipulation. For slip detection, we test the system's reliability on different object geometries and surface textures.

We attach the FORTE fin-ray fingers to a linkage-based gripper and mount the entire gripper assembly to a Franka Emika Panda robot arm. The gripper design is based on the one originally presented in Seo et al. and Yuan et al. [12], [60], which employs Dynamixel XM-430 servos under current-based position control. The position of the servos,  $\theta$ , defines how open / closed the gripper is. We define  $\theta_{\text{closed}} = 0^\circ$  as the servo position when the gripper is fully closed. We define  $\theta_{\text{zeroF}}$  as the servo position when the gripper's fingers *just* touch the object, applying zero force. It means that each object has its own specific  $\theta_{\text{zeroF}}$ , depending on its size.

##### A. Grip Force Estimation

To characterize how well we measure grasp force across different shapes, we perform multiple grasps on custom load-cell testing rigs (Figure 3a). The load cell assembly is vertically and horizontally centered within the gripper's grasp, and a simple *close gripper* operation is performed. By simultaneously measuring the FORTE sensors with the load cell, we can understand how FORTE compares to a ground truth. Figure 3b demonstrates sample data of the FORTE sensor readings against the load cell.

We create the testing rigs by attaching 3D-printed indentors to load cells with a measurement range of 0–50 N. We print indentors in a variety of shapes and sizes to ensure comprehensive coverage of possible object geometries (Figure 4a). The load cells are calibrated with a standard mass of 150g and read out with an Arduino UNO through a 24-bit ADC module (HX711, Adafruit) at 10 Hz.

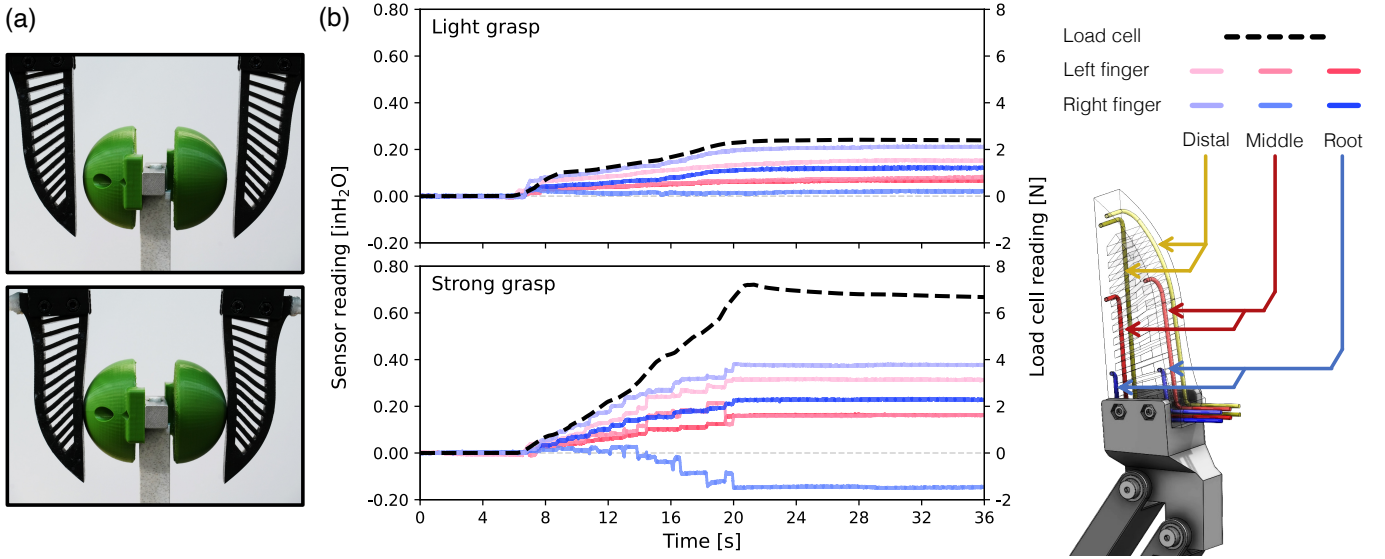


Fig. 3. **Grip Force Data Collection** (a) Snapshots of gripper in open and closed poses during data collection. (b) Sensor and load cell readings over time for a light and strong grip. Red and blue lines show sensor readings from the left and right fingers, respectively, with each line corresponding to a channel pair at distal, middle, or root sensing location. Sensor outputs exhibit a consistent monotonic trend with increasing grip force, with the distal sensors showing the largest response. This trend confirms that the pressure signals scale with finger deformation and support accurate force estimation.

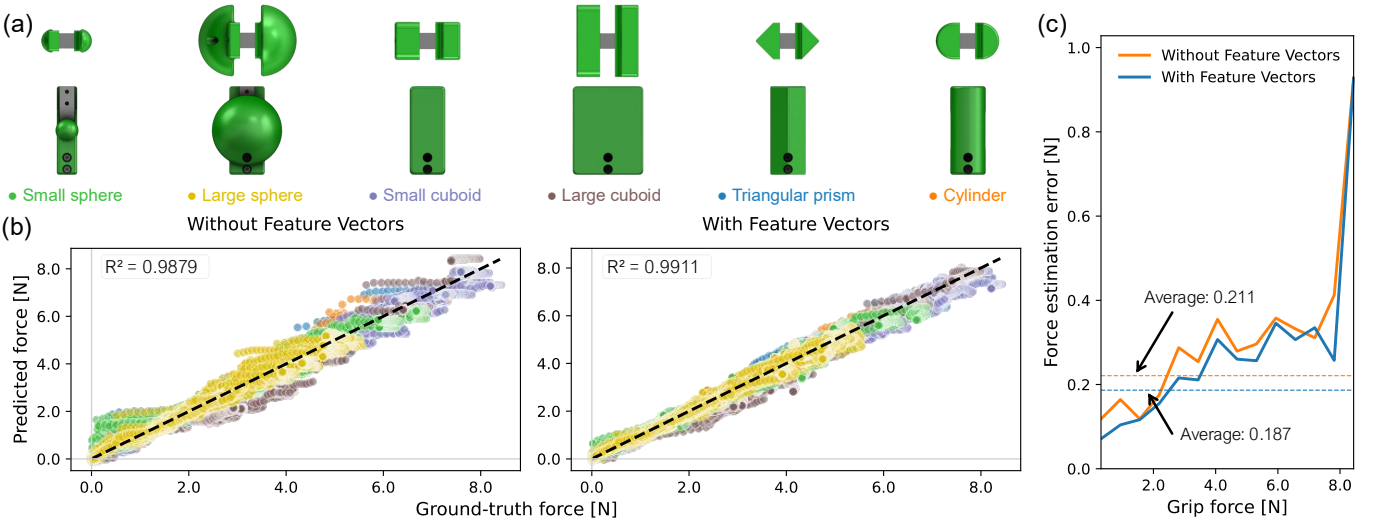


Fig. 4. **Grip Force Estimation Results** (a) Renders of the custom load-cell testing rigs made for grip force data collection. (b) Predicted force versus ground-truth force for models trained without (left) and with (right) the feature vectors from Section III-B as input. Colored dots represent data points collected using the corresponding testing rig, while the dashed black line indicates the line of perfect prediction. (c) Force estimation error as a function of applied grip force. Solid lines show the root mean square error (RMSE) within each force bin, and horizontal dashed lines indicate the overall average error for each condition. Feature vectors reduce the average error from 0.211 N to 0.187 N.

For each of the 6 indentors, we collect data for 40 trials. In each trial, we close the gripper by a random amount, sampling uniformly from “closed” ( $\theta_{\text{closed}} = 0^\circ$ ) to a “just touching” pose ( $\theta_{\text{zeroF}}$ ). This creates a random grasping force against the load cell, which we compare against the FORTE readings. To be specific, the procedure for each trial is as follows:

- 1) Initialize the gripper at open pose (joint positions at  $\frac{\pi}{4}$  rad and collect sensor baselines (5 seconds);
- 2) Close gripper until both fingers just touch the object (load cell measures 0.05 N). Record current joint position as  $\theta_{\text{zeroF}}$  (10 seconds);
- 3) Sample a target joint position  $\hat{\theta} \in [\theta_{\text{zeroF}} -$

$0.02 \text{ rad}, \max(\theta_{\text{zeroF}} - 0.2 \text{ rad}, 0)]$ , then linearly decrease the joint position from  $\theta_{\text{zeroF}}$  to  $\hat{\theta}$  (15 seconds);

- 4) Hold the gripper at  $\hat{\theta}$  (20 seconds);
- 5) Reset the gripper to open pose (10 seconds).

To process each trial, we first normalize each channel’s readings by subtracting the mean of the sensor readings from Step 1 for each channel. We then exclude Step 5 (the reset step) from our data, as we only consider initial contact with the object. As a result, each trial gives us 45 seconds of data. Finally, the sensor readings are filtered with median filters with a kernel size of 11, creating a force estimation dataset of 3 hours with 108k data points. We showcase a sample trial data

cycle for a light and strong grip in Figure 3b.

For both grips, our filtered sensor signals show great correspondence to the grip force, as indicated by the 10-fold trial-wise cross-validation performance of our force estimation algorithm (Figure 4). Across six indenter shapes, our method achieved an average validation RMSE of 0.187. Across six indenter shapes, our method achieved an average RMSE of 0.187 on a force range of 0 to 8 N. The estimation performance surpasses the average error of 0.39 N over a 0.9–4.5 N range reported using a barometric strain gauge array [38], and comparable to the average error of 0.17 N on a force range of 0.3 to 3.0 N using an external camera [23]. This represents a notable improvement over the baseline RMSE of 0.211 obtained without using the feature vector, demonstrating the effectiveness of our approach in enhancing force estimation accuracy.

Figure 4 also demonstrates the importance of using the feature vector  $z(t)$  in conjunction with the pure sensor reading  $S(t)$  to form  $v$  (Section III-B). The use of feature vectors improves regression performance, as the predicted values are more tightly clustered around the perfect prediction line in the scatter plot in Figure 4b. While the increase in cross-validated  $R^2$  from 0.9879 to 0.9911 is not statistically significant, it indicates an overall improvement in model fit with the addition of feature vectors. This improvement is further supported across 16 force range bins as reported in Figure 4c. With feature vectors, the average root mean square error (RMSE) is reduced by 15.6% from 0.221 N to 0.187 N. The improvement is more significant for lower force ranges below 4 N and larger force ranges from 7 N to 8 N, as the sensor history helps alleviate the influence of sensor drifting and gripper material stress relaxation. The estimation error explodes for grip force above 8 N due to a lack of data, as only three trials reached that grip force range. Overall, these results confirm the high-precision force estimation capability of FORTE.

## B. Slip Detection

To characterize slip detection, we generate slip events by attempting to vertically lift an object from the tabletop with insufficient grasping force (Figure 5). Slip detection characterization is not standardized, so we developed our own methods based on the principles from previous work (Section II-C). Our slip generation process created realistic slip events with delicate grip force from the tabletop for the parallel gripper. The only external forces are from gravity and contact with the table, thus requiring no additional constraints and human interference.

To generate the target lift-up motion, we attached the gripper to a Franka Emika Panda robot arm [61]. The robot arm is controlled using Cartesian-space velocity control with Deoxys [62] to generate a vertical lifting trajectory with a constant speed of 1mm/s at 20 Hz. We selected an apple and a jam jar to evaluate slip detection. The apple is widely used to benchmark robotic manipulation [49], [63] due to its curved geometry and inherent fragility. The jam jar features a smooth, slippery surface and a vertical cylindrical shape that forms a narrow, near-line contact under parallel grasping. Although the

jar also has a textured label region, we set the initial grasp to begin with the gripper contacting the slippery and unlabeled portion. The presence of two types of surfaces makes the slip estimation more difficult.

For each object, we define a new servo position:  $\theta_{\text{grasp}}$ , the servo position where the object is stably grasped. For the purposes of characterization, we determine  $\theta_{\text{grasp}}$  by repeatedly lifting the gripper from a fixed pose while gradually decreasing the joint position from  $\theta_{\text{zeroF}}$  until the object is securely lifted.

Once we have defined  $\theta_{\text{grasp}}$ , we use it as a basis for our slip trials. For each trial, we sample a random gripper servo position  $\hat{\theta} \in [\theta_{\text{zeroF}}, \theta_{\text{grasp}}]$ . This will set the force applied by the gripper to be randomly less than the stable grasping force ( $< 0.5$  N), so we know the object will definitely slip. For the apple,  $\hat{\theta} \in [0.552 \text{ rad}, 0.527 \text{ rad}]$ , while for the jam jar,  $\hat{\theta} \in [0.476 \text{ rad}, 0.460 \text{ rad}]$ . We then command the robot arm to vertically lift the gripper at constant velocity. We record this motion and use pixel values from the video to estimate the object’s rotational and translational displacements during slipping. We collect data for 5 trials for each object (Figure 5a).

Upon analysis of the slip data, we first note that the two fingers report different slip results. This is expected as objects are not placed exactly at the midpoint of the gripper workspace, leading to uneven distribution of grasping forces.

For each slip event, we name the finger with the larger contact force as the “leading finger” and the other as the “trailing finger.” Similarly, we name their corresponding contact force as “leading force” and “trailing force.” During a single lifting trial, either the left or right finger may act as the leading finger in different slip events. The information of the leading finger is revealed by the finger-wise moving variance feature as shown in Figure 5d. In the given example, the right finger is the leading finger in slip event 1, while the left finger becomes the leading finger in slip events 2 and 3.

We note that in some cases, the magnitude of the trailing force is superseded by the table friction force. This is because the estimated grip force at  $\theta_{\text{grasp}}$  (0.5 N) is significantly lower than the gravitational force of the apple (2.27 N) and the jam jar (1.42 N). Therefore, we focus on detecting the slip events involving the leading finger, as these are the necessary conditions of gross slip (Section II-B).

We find that our slip detection algorithm can efficiently capture the slip events of transitions from incipient slip to gross slip with a fixed slip threshold  $T = 2 \text{ dB}^2$ . From characterization, we identify two main types of slip events:

- 1) **Leading-Finger Stick-Slip:** Stick-slip occurs at the leading finger while the trailing finger undergoes gross slip.
- 2) **Simultaneous Stick-Slip:** Stick-slip occurs simultaneously at both fingers.

For the first, more common slip type (Leading-Finger Stick-Slip), a significant force imbalance between the leading and trailing fingers causes the trailing finger to slip immediately upon lift, while the leading finger maintains contact. This results in the object tilting, as one side lifts first (Figure 5a). A transition occurs later when the leading finger also begins to slip. For the second, rarer slip type (Simultaneous Stick-Slip),

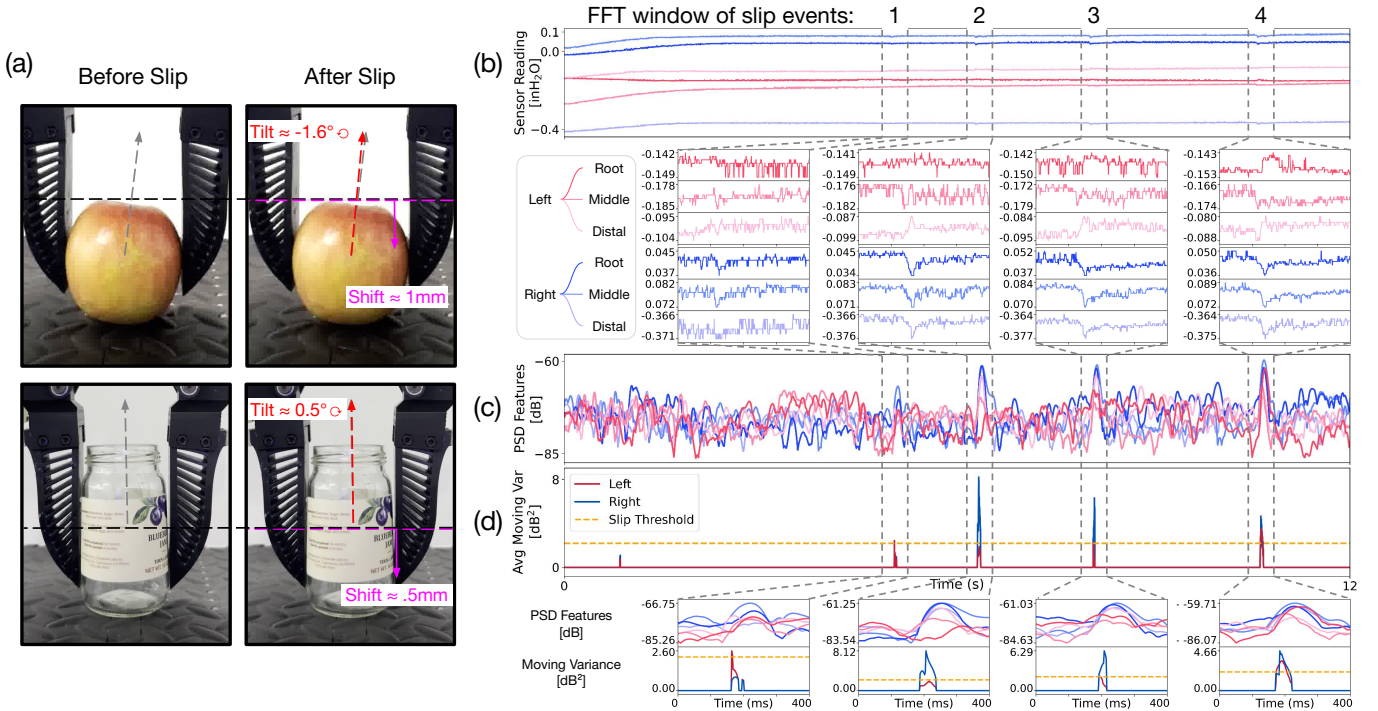


Fig. 5. **Slip Detection Characterization** (a) Snapshots of object displacements caused by stick-slip events. The time difference between the two snapshots of both objects is 66.7 ms. The snapshots of apple corresponds to the slip event 1. (b-d) Filtered sensor readings, PSD features, and average moving variance of one representative trial of lifting an apple. There are four slip events during this trial. At the onset of each slip event, a sharp increase in the PSD feature is observed, resulting in a corresponding spike in the average moving variance, as further illustrated in the zoomed-in views.

fingers begin slipping simultaneously. Slip events of both types can repeat multiple times during a single lifting trial.

The trial of lifting the apple shown in Figure 5 includes both types of slip events. Figure 5b shows the filtered sensor signals as input to our slip detection algorithm. The PSD features computed with Equation. (3) from the FFT windows of size 400 of the filtered sensor signals are shown in Figure 5c. Figure 5d shows the finger-wise average moving variance as the results of Equation. (5).

Comparing Figure 5c and Figure 5d illustrates the effectiveness of measuring the increase in power rather than the magnitude. To be more specific, the first slip event can barely be distinguished from the PSD feature values, while the moving variance cleanly captures the slip event as shown in Figure 5d. Zoomed-in views of the slip events indicate that the latency between the onset of sensor signal change and successful slip detection is consistently below 100 ms. Overall, FORTE enables precise and real-time slip detection.

## V. EXPERIMENTAL SETUP

Now that we have characterized FORTE’s ability to estimate force and detect slip, we would like to know how well FORTE fares in real-world grasping scenarios. In this section, we describe how we will evaluate FORTE against baselines. Our evaluation focuses on the following questions:

- Can FORTE perform single-trial grasping across a wide range of objects, including fragile and slippery ones?
- Can the slip detection algorithm generalize to different objects and conditions?

- How much do force and slip sensing contribute to grasp performance?

We used the gripper setup described in Section III-C and adopted a standardized grasp execution protocol to ensure cross-trial consistency in contact timing, gripping force, and lifting motion. The protocol is detailed below.

- 1) **Initialization:** The gripper is reset to a fixed reference configuration, and its fingers are opened to a predefined starting position. The target object is manually placed between the fingers, with its orientation manually adjusted to introduce variability in initial contact conditions.
- 2) **Object Reaching** The gripper is closed until both fingers make contact with the object. Contact is determined when the maximum absolute change in any of the three tactile signal channels exceeds a threshold  $\tau = 0.5\%$  of full scale span within a sliding window of width  $w = 200$  of 0.1 seconds.
- 3) **Grasp Loading:** After detecting contact, the gripper applies an initial gripping force  $f_{\text{init}} = 0.25$  N, as estimated by the internal force estimator. This ensures a consistent baseline force prior to lift. Note this is around the minimum force threshold we can set given the potential estimation error of around 0.2 N (Figure 4)
- 4) **Slip Detection During Lifting:** Slip detection is enabled, and the gripper begins to lift the object vertically at velocity  $v_{\text{lift}} = 5$  mm/s. As in our slip detection characterization,  $v_{\text{lift}}$  is generated with Cartesian-space velocity control at 20 Hz. If slip is detected during the lift, the gripper command is incremented by  $\Delta_{\text{cmd}} = 0.88^\circ$  to

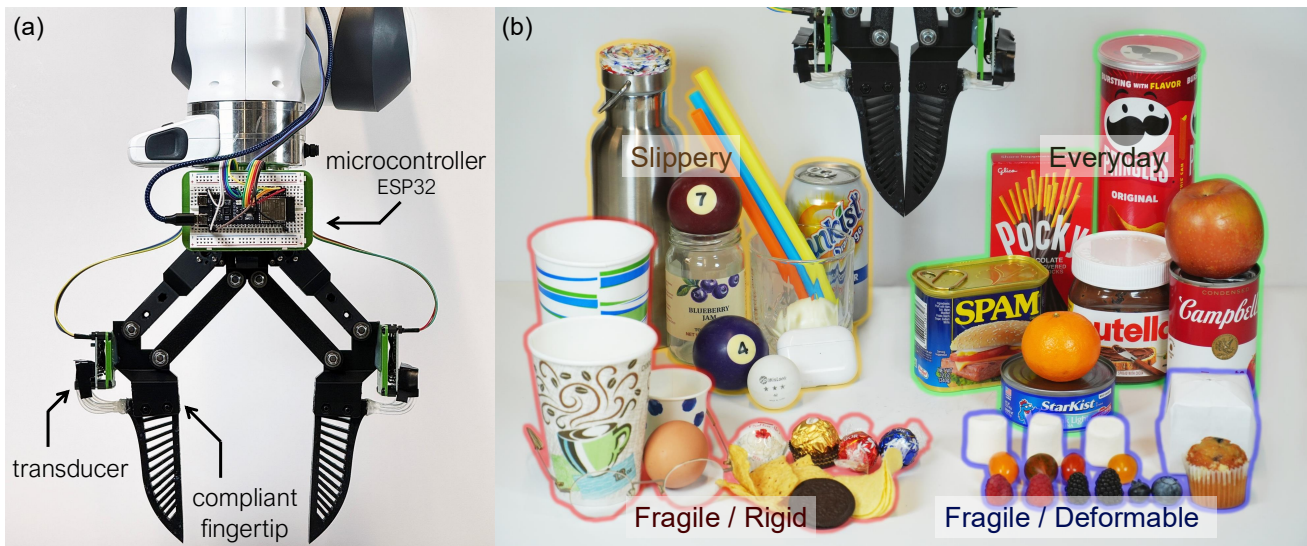


Fig. 6. **Experimental Setup** (a) FORTE is mounted on a Franka Emika Panda robot arm for table-top grasping tests. (b) Objects used for evaluation. Fragile objects are selected to evaluate force estimation accuracy and gripper compliance, while slippery items and eight everyday YCB objects are chosen to assess slip detection performance.

increase the applied force and counteract the slip.

- 5) **Lift Completion Criteria:** The gripper continues lifting until the object is either successfully elevated off the support surface or dropped due to grasp failure.

On FORTE, the force estimation module operates at 100 Hz with an update latency of less than 10 ms, providing timely feedback for closed-loop control. The slip detection algorithm runs at 500 Hz as determined by the selected signal window size of 400 and an overlap factor of 0.99, and the typical detection latency is below 100 ms.

We compare FORTE against two baseline conditions:

- **On-Off:** After initialization, the gripper closes at the same speed as in the object-reaching step until fully closed, then lifts the object without any slip detection. This baseline reflects only the ability of the compliant fingers and provides a reference without using any feedback.
- **W/o Slip:** Follows the full grasping protocol but disables slip detection during the lifting phase. This baseline uses a fixed force without reactive adjustment, allowing us to evaluate the importance of slip detection.

We evaluated FORTE and the baselines through a 31-item test set with 4 specific categories of interest: fragile and rigid objects, fragile and deformable objects, slippery objects, and everyday objects (Figure 6). Items are drawn from real-world environments and the YCB food items [63]. We conducted experiments of 10 independent trials for each of the objects on a set of 47 object instances across the 31 distinct object types (Table II).

## VI. EXPERIMENTAL RESULTS

In this section, we report how well FORTE performs under real grasping conditions. Results are presented in Table II. With force and slip sensing enabled by our solution, we can achieve a success rate of 91.9% among all the 310 trials.

Meanwhile, the two baselines On-Off and W/o Slip can only achieve 60% and 52.6% success rates. We would like to emphasize that our high success rate is achieved in *single-trial* experiments. The slip detection threshold  $T$  is set only by the apple and jam jar used for characterization, so the majority of these objects are unseen and out of distribution. This suggests that our slip detection algorithm generalizes by capturing shared signal patterns of slip events, without relying on object-specific calibration.

### A. Grasping Results

We evaluate the success of our force-sensing capabilities by examining how well Fragile objects are handled. Since we command FORTE to use a gentle initial gripping force of 0.25 N, 13 out of 14 fragile objects are able to be lifted with a 100% success rate. By contrast, the simple On-Off controller broke the surface of 8 out of the 14 selected objects and caused unrecoverable deformation of the blueberry, grape, tomato, and marshmallow. We do note that the On-Off controller had a 100% success rate on the Raw Egg and the Chocolate Ball. A traditional rigid gripper with an On-Off controller would likely break both of these objects, highlighting how important it is to make FORTE compliant.

We evaluate the success of our slip-detecting capabilities by examining how well Slippery and Everyday Objects are handled. In the W/o Slip baseline, 15 out of the 17 objects of the two categories are not able to be reliably lifted with the initial gripping force. By contrast, FORTE’s use of adaptive grasping with slip detection while lifting resulted in a 100% success rate for 10 out of the 15 objects. This is especially notable with the 8 everyday objects selected from the YCB dataset [63]. The W/o Slip baseline only achieves a 1.25% success rate, while FORTE achieves an 85% success rate. The sole failure that the W/o Slip controller had in lifting the Nutella jar is due to incorrect force prediction, caused by the object being placed too far off-center during initialization.

TABLE II  
SUMMARY OF SLIP-DETECTION METRICS AND GRASP SUCCESS RATE FOR 31 OBJECT TYPES, CATEGORIZED INTO FOUR SEMANTIC GROUPS.

Category	Object (Weight (g))	# of Trials with Slip	True Positives	True Negatives	False Positives	On-Off Baseline	W/o Slip Baseline	FORTE
<b>Fragile / Rigid</b> (7 objects)	Oreo Thins (7)	0	0	10	0	✗	10/10	10/10
	Raw Egg (62-64)	5	3	5	0	10/10	4/10	8/10
	Tortilla Chip (3-5)	0	0	10	0	✗	10/10	10/10
	Potato Chip (2)	0	0	10	0	✗	10/10	10/10
	Chocolate Ball (10-11)	0	0	10	0	10/10	10/10	10/10
	Eye-glasses (11)	0	0	10	0	N/A	10/10	10/10
	Paper Cup (2,11,20)	0	0	10	0	✗	10/10	10/10
<i>Category Success Rate</i>						33.3% (20/60)	91.4% (64/70)	<b>97.1%</b> <b>(68/70)</b>
<i>Slip Detection Metrics</i>		Accuracy 0.97	Precision 1.00	Recall 0.60	F1 Score 0.75			
<b>Fragile / Deformable</b> (7 objects)	Origami Ball	0	0	10	0	✗	10/10	10/10
	Raspberry (3-4)	0	0	10	0	✗	10/10	10/10
	Blackberry (4-5)	0	0	10	0	✗	10/10	10/10
	Blueberry (1-2)	0	0	10	0	Oversqueeze	10/10	10/10
	Grape Tomato (10-15)	0	0	10	0	Oversqueeze	10/10	10/10
	Marshmallow (4-6)	0	0	10	0	Oversqueeze	10/10	10/10
	Muffin (24-26)	0	0	10	0	✗	10/10	10/10
<i>Category Success Rate</i>						0% (0/70)	<b>100%</b> <b>(70/70)</b>	<b>100%</b> <b>(70/70)</b>
<i>Slip Detection Metrics</i>		Accuracy 1.00	Precision 1.00	Recall 0.00	F1 Score 0.00			
<b>Slippery</b> (9 objects)	Jam Jar (145)	8	8	2	0	10/10	0/10	10/10
	Whiskey Cup (278)	10	10	0	0	10/10	0/10	10/10
	Ping-pong Ball (3)	0	0	10	0	10/10	10/10	10/10
	Billiard Ball (170)	10	10	0	0	10/10	0/10	10/10
	Straw (1)	0	0	10	0	10/10	10/10	10/10
	Air-pod Case (61)	2	2	8	0	10/10	8/10	10/10
	Soda (371)	10	10	0	0	10/10	0/10	10/10
	Metal Bottle (299)	10	10	0	0	10/10	0/10	10/10
	Hard-boiled Egg (52)	10	0	0	0	0/10	0/10	0/10
<i>Category Success Rate</i>						<b>88.8%</b> <b>(80/90)</b>	31.1% (28/90)	<b>88.8%</b> <b>(80/90)</b>
<i>Slip Detection Metrics</i>		Accuracy 0.91	Precision 1.00	Recall 0.82	F1 Score 0.90			
<b>Everyday</b> (8 objects)	Pringles (197)	10	10	0	0	10/10	0/10	9/10
	Nutella (311)	10	10	0	0	10/10	1/10	10/10
	Tuna Can (178)	10	10	0	0	10/10	0/10	10/10
	Campbell Soup (348)	10	10	0	0	10/10	0/10	10/10
	Mandarin (88-96)	10	10	0	0	10/10	0/10	10/10
	Apple (231)	10	9	0	0	10/10	0/10	9/10
	SPAM (368)	10	10	0	0	10/10	0/10	10/10
	Pocky Box (88)	10	0	0	0	10/10	0/10	0/10
<i>Category Success Rate</i>						<b>100%</b> <b>(80/80)</b>	1.25% (1/80)	85.0% (68/80)
<i>Slip Detection Metrics</i>		Accuracy 0.88	Precision 1.00	Recall 0.86	F1 Score 0.93			
<b>Overall Success Rate</b>						60% (180/300)	52.6% (163/310)	<b>91.9%</b> <b>(285/310)</b>
<b>Overall Slip Detection Metrics</b>		0.93	1.00	0.84	0.91			

None of the three tested methods are able to lift hard-boiled eggs. FORTE and W/o Slip failed due to insufficient gripping force, while the On-Off baseline slowly squeezed the egg out of the gripper. It is noteworthy that for the Pringles, slippage is detected for all the trials, yet we still dropped the object during one of the trials. In this trial, the canister is initialized on the table lying sideways, and the fingers reach from the side to grasp its lateral surface. Multiple slip events

are detected throughout the whole procedure, including the last slip event that causes the Pringles bottle to fall out of the gripper. However, the gripper control is not responsive enough to catch the falling bottle when the grasp is achieved with the distal regions of the fingers. This implies that further work must be done to improve the responsiveness of the FORTE system for future real-world applications.

In conclusion, FORTE demonstrates strong generalization

across fragile, slippery, and everyday objects by combining a compliant finger with real-time force estimation and slip detection. These results underscore FORTE’s effectiveness in delicate manipulation, setting a solid foundation for more responsive robotic manipulation in real-world settings.

### B. Slip Detection Performance

In addition to grasping performance, we would like to evaluate how accurate our slip detection algorithm is in real-world grasping. We record how many trials had slips during lifting and then report how many true positive, true negative, and false positive slip predictions are made. We also report summary statistics of accuracy, precision, recall, and the F1 score (Table II). When both ground truth slippage and predicted slippage are 0, precision is mathematically undefined; we define the precision in such a case as 1.0 to reflect the algorithm’s correct abstention from false positives.

The slip detection algorithm achieves an overall trial-wise accuracy of 0.93 and an F1 score of 0.91. The precision of our slip detection algorithm of 1 across all 310 trials demonstrates the trustworthiness of our slip detection algorithm. This high precision avoids unnecessary grasp adjustments and results in a high success rate of 98.6% for grasping the 14 selected fragile objects.

Since our slip detection algorithm targets the stick-slip events as discussed in Section IV-B, typical failure cases arise when the applied gripping force is too low to generate detectable contact interactions between the finger surface and the object. The slip detector failed to detect the slippage of the hard-boiled egg and the Pocky box, since these two objects have a very low friction coefficient between the object surface and FORTE’s fingers. Smooth and continuous gross slip initiates at the beginning of lifting, and the transition is not significant enough to generate a detectable power increase of PSD features. Similarly, among the 20 trials of grasping raw eggs and apples, our slip detection algorithm made 3 false negative predictions. In all three trials, the objects rolled out from the side of the gripper as rotational gross slip is initiated. This is primarily caused by the small contact area between the edge of the finger surface and the objects’ curved geometry, together with their off-centered center of mass.

In addition to the two types of targeted slip events defined in Section IV-B, we identified two other types of slip events during gross slip that can be captured with our slip detection algorithm:

- 1) **Rotational-to-Translational Slip Transition:** Slip begins as rotational gross slip and transitions into translational gross slip during lifting.
- 2) **Texture-Affected Slip:** Local surface texture variations cause detectable fingertip deformation during gross slip.

A typical case of rotational-to-translational slip transition includes side gripping at the off-centered position of objects of elongated geometries, such as the Pringles Bottle and the Metal Bottle. As one end of the bottle is lifted and the object tilts more gradually, translational gross slip will be initiated. A representative example of texture-affected slip is when slip is detected as the fingertip moves across the circumferential

ridges along the side of a tomato soup can. Further work is needed to improve our algorithm to better capture these more differentiated types of slip events.

Overall, our slip detection algorithm demonstrates robust performance across unseen and diverse objects, with sufficient responsiveness to detect and react to slippage during lifting. Moreover, it captures multiple types of slip events through a unified analytical approach. This capability is essential for achieving delicate manipulation in real-world robotic applications.

## VII. DISCUSSION

In this work, we introduced a system that integrates force and slip sensing into compliant robotic fingers with simple 3D-printing-based manufacturing. This combination enables a parallel gripper to perform delicate manipulation tasks, such as handling fragile objects like raspberries and potato chips. Leveraging accurate slip detection with a real-world accuracy of 0.91, our system achieves a single-trial grasping success rate of 91.9% over 31 diverse objects.

One notable limitation of FORTE is that the sensor signal is sensitive to temperature change on the finger surface. According to the ideal gas law  $PV = nRT$ , a rise in temperature  $T$  will only increase the internal pressure  $P$  in the sealed air channels under the inner finger surface, and vice versa. This temperature-induced pressure variation introduces large-magnitude noise into the sensor readings and can cause the system to respond inconsistently to identical contact and slip events. This limitation can possibly be improved with a more advanced design of channel geometry and layout.

While our slip detection algorithm effectively captures various types of slip events, it shares a common limitation of frequency-domain-based methods that continuous gross slip on low-friction surfaces is difficult to detect. Future direction includes adding stimulus shapes on the surface of the fingers and incorporating other sensing modalities.

In addition, our current servo control frequency of 25 Hz is significantly lower than the sampling rates used for force estimation (100 Hz) and slip detection (400 Hz). This limits the system’s ability to react quickly to changes during manipulation. A higher control frequency would allow more precise and responsive gripper movements, better demonstrating the capability of FORTE. Overall, FORTE presents a compelling solution for integrating force and slip sensing to compliant gripper fingers.

## REFERENCES

- [1] S. L. Gorniak, V. M. Zatsiorsky, and M. L. Latash, "Manipulation of a fragile object," *Experimental brain research*, vol. 202, pp. 413–430, 2010.
- [2] A. Kumar, Y. Tanaka, A. Grigoriadis, J. Grigoriadis, M. Trullsson, and P. Svensson, "Training-induced dynamics of accuracy and precision in human motor control," *Scientific reports*, vol. 7, no. 1, p. 6784, 2017.
- [3] H. E. Wheat, L. M. Salo, and A. W. Goodwin, "Human ability to scale and discriminate forces typical of those occurring during grasp and manipulation," *Journal of Neuroscience*, vol. 24, no. 13, pp. 3394–3401, 2004.
- [4] G. Westling and R. S. Johansson, "Responses in glabrous skin mechanoreceptors during precision grip in humans," *Experimental brain research*, vol. 66, no. 1, pp. 128–140, 1987.
- [5] R. S. Johansson and Åke B. Vallbo, "Tactile sensory coding in the glabrous skin of the human hand," *Trends in Neurosciences*, vol. 6, pp. 27–32, 1983.
- [6] R. S. Johansson and G. Westling, "Roles of glabrous skin receptors and sensorimotor memory in automatic control of precision grip when lifting rougher or more slippery objects," *Experimental brain research*, vol. 56, no. 3, pp. 550–564, 1984.
- [7] R. S. Johansson and J. R. Flanagan, "Coding and use of tactile signals from the fingertips in object manipulation tasks," *Nature Reviews Neuroscience*, vol. 10, no. 5, pp. 345–359, 2009.
- [8] T. Z. Zhao, J. Tompson, D. Driess, P. Florence, K. Ghasemipour, C. Finn, and A. Wahid, "Aloha unleashed: A simple recipe for robot dexterity," *arXiv preprint arXiv:2410.13126*, 2024.
- [9] C. Chi, Z. Xu, S. Feng, E. Cousineau, Y. Du, B. Burchfiel, R. Tedrake, and S. Song, "Diffusion policy: Visuomotor policy learning via action diffusion," *The International Journal of Robotics Research*, p. 02783649241273668, 2023.
- [10] K. Black, N. Brown, D. Driess, A. Esmail, M. Equi, C. Finn, N. Fusai, L. Groom, K. Hausman, B. Ichter *et al.*, "*pi*\_0: A vision-language-action flow model for general robot control," *arXiv preprint arXiv:2410.24164*, 2024.
- [11] J. Bjorck, F. Castañeda, N. Cherniadev, X. Da, R. Ding, L. Fan, Y. Fang, D. Fox, F. Hu, S. Huang *et al.*, "Gr00t n1: An open foundation model for generalist humanoid robots," *arXiv preprint arXiv:2503.14734*, 2025.
- [12] M. Seo, H. A. Park, S. Yuan, Y. Zhu, and L. Sentis, "Legato: Cross-embodiment imitation using a grasping tool," *IEEE Robotics and Automation Letters (RA-L)*, 2025.
- [13] T. Z. Zhao, V. Kumar, S. Levine, and C. Finn, "Learning fine-grained bimanual manipulation with low-cost hardware," *arXiv preprint arXiv:2304.13705*, 2023.
- [14] C. Chi, Z. Xu, C. Pan, E. Cousineau, B. Burchfiel, S. Feng, R. Tedrake, and S. Song, "Universal manipulation interface: In-the-wild robot teaching without in-the-wild robots," *arXiv preprint arXiv:2402.10329*, 2024.
- [15] P. Wu, Y. Shentu, Q. Liao, D. Jin, M. Guo, K. Sreenath, X. Lin, and P. Abbeel, "Robocopilot: Human-in-the-loop interactive imitation learning for robot manipulation," *arXiv preprint arXiv:2503.07771*, 2025.
- [16] W. Crooks, G. Vukasin, M. O'Sullivan, W. Messner, and C. Rogers, "Fin ray@ effect inspired soft robotic gripper: From the robosoft grand challenge toward optimization," *Frontiers in Robotics and AI*, vol. 3, p. 70, 2016.
- [17] C. Della Santina *et al.*, "Dexterity augmentation on a synergistic hand: the pisa/iit sothand+," in *Proceedings of the 2015 IEEE-RAS International Conference on Humanoid Robots (Humanoids)*. IEEE, 2015, pp. 497–503.
- [18] R. A. Romeo and L. Zollo, "Methods and sensors for slip detection in robotics: A survey," *Ieee Access*, vol. 8, pp. 73 027–73 050, 2020.
- [19] W. Chen, H. Khamis, I. Birznieks, N. F. Lepora, and S. J. Redmond, "Tactile sensors for friction estimation and incipient slip detection—toward dexterous robotic manipulation: A review," *IEEE Sensors Journal*, vol. 18, no. 22, pp. 9049–9064, 2018.
- [20] S. Q. Liu and E. H. Adelson, "Gelsight fin ray: Incorporating tactile sensing into a soft compliant robotic gripper," in *2022 IEEE 5th International Conference on Soft Robotics (RoboSoft)*. IEEE, 2022, pp. 925–931.
- [21] Y. Wang, H. Wu, H. Guo, and H. Dong, "Gelsight flexiray: Breaking planar limits by harnessing large deformations for flexible,full-coverage multimodal sensing," 2024. [Online]. Available: <https://arxiv.org/abs/2411.18979>
- [22] A. Zhang, R. L. Truby, L. Chin, S. Li, and D. Rus, "Vision-based sensing for electrically-driven soft actuators," *IEEE Robotics and Automation Letters*, vol. 7, no. 4, pp. 11 509–11 516, 2022.
- [23] W. Xu, H. Zhang, H. Yuan, and B. Liang, "A compliant adaptive gripper and its intrinsic force sensing method," *IEEE Transactions on Robotics*, vol. 37, no. 5, pp. 1584–1603, 2021.
- [24] B. Shih, D. Drotman, C. Christianson, Z. Huo, R. White, H. I. Christensen, and M. T. Tolley, "Custom soft robotic gripper sensor skins for haptic object visualization," in *2017 IEEE/RSSJ international conference on intelligent robots and systems (IROS)*. IEEE, 2017, pp. 494–501.
- [25] J. Hashizume, T. M. Huh, S. A. Suresh, and M. R. Cutkosky, "Capacitive sensing for a gripper with gecko-inspired adhesive film," *IEEE Robotics and Automation Letters*, vol. 4, no. 2, pp. 677–683, 2019.
- [26] A. Pagoli, F. Chapelle, J.-A. Corrales-Ramon, Y. Mezouar, and Y. Lapusta, "Large-area and low-cost force/tactile capacitive sensor for soft robotic applications," *Sensors*, vol. 22, no. 11, p. 4083, 2022.
- [27] F. Qi, L. Xu, Y. He, H. Yan, and H. Liu, "Pvd-f based flexible piezoelectric tactile sensors," *Crystal Research and Technology*, vol. 58, no. 10, p. 2300119, 2023.
- [28] W. Diao, X. Wang, W. Shi, Y. Cao, and G. Liu, "A tribo-piezoelectric coupled sensor for force and slip detection in soft grippers," *Nano Energy*, p. 110697, 2025.
- [29] S. Q. Liu, *Soft, Compliant Tactile Robotic Manipulators*. Massachusetts Institute of Technology, 2024.
- [30] N. Kuppuswamy, A. Alspach, A. Uttamchandani, S. Creasey, T. Ikeda, and R. Tedrake, "Soft-bubble grippers for robust and perceptive manipulation," in *2020 IEEE/RSSJ International Conference on Intelligent Robots and Systems (IROS)*. IEEE, 2020, pp. 9917–9924.
- [31] G. Zöllner, V. Wall, and O. Brock, "Active acoustic contact sensing for soft pneumatic actuators," in *2020 IEEE International Conference on Robotics and Automation (ICRA)*. IEEE, 2020, pp. 7966–7972.
- [32] V. Wall, G. Zöllner, and O. Brock, "Passive and active acoustic sensing for soft pneumatic actuators," *The International Journal of Robotics Research*, vol. 42, no. 3, pp. 108–122, 2023.
- [33] Z. Liu, C. Chi, E. Cousineau, N. Kuppuswamy, B. Burchfiel, and S. Song, "Maniway: Learning robot manipulation from in-the-wild audio-visual data," in *8th Annual Conference on Robot Learning*, 2024.
- [34] L. He, Q. Lu, S.-A. Abad, N. Rojas, and T. Nanayakkara, "Soft fingertips with tactile sensing and active deformation for robust grasping of delicate objects," *IEEE Robotics and Automation letters*, vol. 5, no. 2, pp. 2714–2721, 2020.
- [35] R. L. Truby, L. Chin, A. Zhang, and D. Rus, "Fluidic innervation sensorized structures from a single build material," *Science advances*, vol. 8, no. 31, p. eabq4385, 2022.
- [36] A. Zhang, L. Chin, D. L. Tong, and D. Rus, "Embedded air channels transform soft lattices into sensorized grippers," in *2024 IEEE International Conference on Robotics and Automation (ICRA)*. IEEE, 2024, pp. 5264–5270.
- [37] A. M. Gruebele, M. A. Lin, D. Brouwer, S. Yuan, A. C. Zerbe, and M. R. Cutkosky, "A stretchable tactile sleeve for reaching into cluttered spaces," *IEEE Robotics and Automation Letters*, vol. 6, no. 3, pp. 5308–5315, 2021.
- [38] H. Choi, M. R. Cutkosky, and A. A. Stanley, "Integrated pneumatic sensing and actuation for soft haptic devices," *IEEE Robotics and Automation Letters*, vol. 8, no. 11, pp. 7591–7598, 2023.
- [39] R. D. Howe and M. R. Cutkosky, "Sensing skin acceleration for slip and texture perception," in *ICRA*, 1989, pp. 145–150.
- [40] J. Byerlee, "The mechanics of stick-slip," *Tectonophysics*, vol. 9, no. 5, pp. 475–486, 1970.
- [41] S. Dong, D. Ma, E. Donlon, and A. Rodriguez, "Maintaining grasps within slipping bounds by monitoring incipient slip," in *2019 International Conference on Robotics and Automation (ICRA)*. IEEE, 2019, pp. 3818–3824.
- [42] J. Li, S. Dong, and E. Adelson, "Slip detection with combined tactile and visual information," in *2018 IEEE International Conference on Robotics and Automation (ICRA)*. IEEE, 2018, pp. 7772–7777.
- [43] A. Rigi, F. Baghaei Naeini, D. Makris, and Y. Zweiri, "A novel event-based incipient slip detection using dynamic active-pixel vision sensor (davis)," *Sensors*, vol. 18, no. 2, p. 333, 2018.
- [44] R. Muthusamy, X. Huang, Y. Zweiri, L. Seneviratne, and D. Gan, "Neuromorphic event-based slip detection and suppression in robotic grasping and manipulation," *IEEE Access*, vol. 8, pp. 153 364–153 384, 2020.
- [45] N. Funk, E. Helmut, G. Chalvatzaki, R. Calandra, and J. Peters, "Evetac: An event-based optical tactile sensor for robotic manipulation," *IEEE Transactions on Robotics*, 2024.
- [46] G. Kim and D. Hwang, "Barotac: Barometric three-axis tactile sensor with slip detection capability," *Sensors*, vol. 23, no. 1, p. 428, 2022.

- [47] Y. Li, M. Zhao, Y. Yan, L. He, Y. Wang, Z. Xiong, S. Wang, Y. Bai, F. Sun, Q. Lu *et al.*, “Multifunctional biomimetic tactile system via a stick-slip sensing strategy for human–machine interactions,” *NPJ Flexible electronics*, vol. 6, no. 1, p. 46, 2022.
- [48] Z. Su, K. Hausman, Y. Chebotar, A. Molchanov, G. E. Loeb, G. S. Sukhatme, and S. Schaal, “Force estimation and slip detection/classification for grip control using a biomimetic tactile sensor,” in *2015 IEEE-RAS 15th International Conference on Humanoid Robots (Humanoids)*. IEEE, 2015, pp. 297–303.
- [49] J. M. Romano, K. Hsiao, G. Niemeyer, S. Chitta, and K. J. Kuchenbecker, “Human-inspired robotic grasp control with tactile sensing,” *IEEE Transactions on Robotics*, vol. 27, no. 6, pp. 1067–1079, 2011.
- [50] R. Fernandez, I. Payo, A. S. Vazquez, and J. Becedas, “Micro-vibration-based slip detection in tactile force sensors,” *Sensors*, vol. 14, no. 1, pp. 709–730, 2014.
- [51] M. Schöpfer, C. Schürmann, M. Pardowitz, and H. Ritter, “Using a piezo-resistive tactile sensor for detection of incipient slippage,” in *ISR 2010 (41st International Symposium on Robotics) and ROBOTIK 2010 (6th German Conference on Robotics)*. VDE, 2010, pp. 1–7.
- [52] M. Meier, F. Patzelt, R. Haschke, and H. J. Ritter, “Tactile convolutional networks for online slip and rotation detection,” in *Artificial Neural Networks and Machine Learning–ICANN 2016: 25th International Conference on Artificial Neural Networks, Barcelona, Spain, September 6–9, 2016, Proceedings, Part II 25*. Springer, 2016, pp. 12–19.
- [53] F. Veiga, H. Van Hoof, J. Peters, and T. Hermans, “Stabilizing novel objects by learning to predict tactile slip,” in *2015 IEEE/RSJ International Conference on Intelligent Robots and Systems (IROS)*. IEEE, 2015, pp. 5065–5072.
- [54] J. W. James and N. F. Lepora, “Slip detection for grasp stabilization with a multifingered tactile robot hand,” *IEEE Transactions on Robotics*, vol. 37, no. 2, pp. 506–519, 2020.
- [55] F. Veiga, J. Peters, and T. Hermans, “Grip stabilization of novel objects using slip prediction,” *IEEE transactions on haptics*, vol. 11, no. 4, pp. 531–542, 2018.
- [56] C. Zhao, Y. Yu, Z. Ye, Z. Tian, Y. Zhang, and L.-L. Zeng, “Universal slip detection of robotic hand with tactile sensing,” *Frontiers in Neuro-robotics*, vol. 19, p. 1478758, 2025.
- [57] X. Hu, A. Venkatesh, G. Zheng, and X. Chen, “Learning to detect slip through tactile measures of the contact force field and its entropy,” *arXiv preprint arXiv:2303.00935*, 2023.
- [58] J. Shintake, V. Cacucciolo, D. Floreano, and H. Shea, “Soft robotic grippers,” *Advanced materials*, vol. 30, no. 29, p. 1707035, 2018.
- [59] M. H. Ali, A. Zhanabayev, S. Khamzhin, and K. Mussin, “Biologically inspired gripper based on the fin ray effect,” in *2019 5th International Conference on Control, Automation and Robotics (ICCAR)*. IEEE, 2019, pp. 865–869.
- [60] S. Yuan, S. Wang, R. Patel, M. Tippur, C. L. Yako, M. R. Cutkosky, E. Adelson, and K. Salisbury, “Tactile-reactive roller grasper,” *IEEE Transactions on Robotics*, 2025.
- [61] “Franka Robotics,” <https://franka.de/>.
- [62] Y. Zhu, A. Joshi, P. Stone, and Y. Zhu, “Viola: Imitation learning for vision-based manipulation with object proposal priors,” *arXiv preprint arXiv:2210.11339*, 2022.
- [63] B. Calli, A. Singh, J. Bruce, A. Walsman, K. Konolige, S. Srinivasa, P. Abbeel, and A. M. Dollar, “Yale-cmu-berkeley dataset for robotic manipulation research,” *The International Journal of Robotics Research*, vol. 36, no. 3, pp. 261–268, 2017.